Received: 14 March 2023 | Revised: 23 August 2023 | Accepted: 28 August 2023

DOI: 10.1111/bph.16250

RESEARCH ARTICLE

The impact of uncertainty in hERG binding mechanism on in silico predictions of drug-induced proarrhythmic risk

Chon Lok Lei[1,2] | Dominic G. Whittaker[3] | Gary R. Mirams[3]

[1]Institute of Translational Medicine, Faculty of Health Sciences, University of Macau, Macau, China

[2]Department of Biomedical Sciences, Faculty of Health Sciences, University of Macau, Macau, China

[3]Centre for Mathematical Medicine & Biology, School of Mathematical Sciences, University of Nottingham, Nottingham, UK

Correspondence
Gary R. Mirams, Centre for Mathematical Medicine & Biology, School of Mathematical Sciences, University of Nottingham, Nottingham, UK.
Email: gary.mirams@nottingham.ac.uk

Present address
Dominic G. Whittaker, Systems Modeling & Translational Biology, GSK, Stevenage, UK.

Funding information
This work was supported by the Wellcome Trust [grant no. 212203/Z/18/Z]; the Science and Technology Development Fund, Macao SAR (FDCT) [reference no. 0048/2022/A]. GRM and DGW acknowledge support from the Wellcome Trust via a Senior Research Fellowship to GRM. CLL acknowledges support from the FDCT and support from the University of Macau via a UM Macao Fellowship. This work was performed in part at the high performance computing cluster (HPCC) supported by the Information and Communication Technology Office (ICTO) of the University of Macau. This research was funded in whole, or in part, by the Wellcome Trust [212203/Z/18/Z]. For the purpose of open access, the authors have applied a CC-BY public copyright licence to any Author Accepted Manuscript version arising from this submission.

Abstract

Background and Purpose: Drug-induced reduction of the rapid delayed rectifier potassium current carried by the human Ether-à-go-go-Related Gene (hERG) channel is associated with increased risk of arrhythmias. Recent updates to drug safety regulatory guidelines attempt to capture each drug's hERG binding mechanism by combining in vitro assays with in silico simulations. In this study, we investigate the impact on in silico proarrhythmic risk predictions due to uncertainty in the hERG binding mechanism and physiological hERG current model.

Experimental Approach: Possible pharmacological binding models were designed for the hERG channel to account for known and postulated small molecule binding mechanisms. After selecting a subset of plausible binding models for each compound through calibration to available voltage-clamp electrophysiology data, we assessed their effects, and the effects of different physiological models, on proarrhythmic risk predictions.

Key Results: For some compounds, multiple binding mechanisms can explain the same data produced under the safety testing guidelines, which results in different inferred binding rates. This can result in substantial uncertainty in the predicted torsade risk, which often spans more than one risk category. By comparison, we found that the effect of a different hERG physiological current model on risk classification was subtle.

Conclusion and Implications: The approach developed in this study assesses the impact of uncertainty in hERG binding mechanisms on predictions of drug-induced proarrhythmic risk. For some compounds, these results imply the need for additional binding data to decrease uncertainty in safety-critical applications.

KEYWORDS
binding mechanism, CiPA, hERG, mathematical modelling, proarrhythmic risk, safety pharmacology, torsade

1 | INTRODUCTION

The human Ether-à-go-go-Related Gene (hERG) encodes the pore-forming alpha subunit of the ion channel $K_V11.1$ that conducts

Abbreviations: AP, action potential; APD_{90}, action potential duration at 90% repolarisation; CiPA, Comprehensive in-vitro Pro-arrhythmia Assay (www.cipaproject.org); HEK293, human embryonic kidney cell line 293; hERG, human Ether-à-go-go-Related Gene; RMSD, root mean square difference.

I_{Kr} (Sanguinetti et al., 1995). The hERG channel is highly susceptible to blockage or functional inhibition by a variety of pharmaceutical small molecules (Sanguinetti & Tristani-Firouzi, 2006; Vandenberg et al., 2012), we simply refer to these as 'compounds' throughout. Reduction of the rapid delayed rectifier potassium current, I_{Kr}, can lengthen the action potential (AP), which is associated with increased risk of cardiac arrhythmias, including Torsade de Pointes (Curran et al., 1995; Heist & Ruskin, 2010), although this risk is strongly modulated by multichannel block (Mirams et al., 2011). In vitro studies including hERG are part of the regulatory guidelines for proarrhythmic risk assessment of novel compounds (ICH, 2005). Recently, the Comprehensive in-vitro Proarrhythmia Assay (CiPA) initiative and updates of regulatory guidelines consider a more nuanced characterisation of a drug's proarrhythmic potential, by combining in vitro assays for multiple ion channels with in silico simulations. For hERG, this approach examines the details of each compound's binding mechanism, particularly the degree to which each compound is trapped (cannot unbind) when the channel closes (ICH, 2022; Li et al., 2019; Sager et al., 2014).

The inner cavity of the hERG channel is its principal drug compound binding site (Mitcheson, 2008). The molecular structure of the channel suggests that compounds only bind when channels are not closed (Butler et al., 2020), consistent with the observation that most of the compounds do not bind at negative (resting/repolarised) membrane potentials when hERG channels are in a nonconducting closed state (Li et al., 2017). After binding to the channel, compounds may also unbind when channels are in different states and/or at different voltages (Mitcheson et al., 2000; Thouta et al., 2018). However, the unbinding process for some compounds can be impeded when the channels close, and the compounds remain bound, or 'trapped' within the central cavity (Mitcheson et al., 2000; Stork et al., 2007; Thouta et al., 2018; Windisch et al., 2011), such as **bepridil** (Pareja et al., 2013) and **dofetilide** (Milnes et al., 2010), as opposed to, for example, **cisapride** (Milnes et al., 2010) and **verapamil** (S. Zhang et al., 1999), which unbind when the chancels close. According to the modulated receptor hypothesis, the difference in affinity determines the preferential binding of a compound to one of the states (Carmeliet & Mubagwa, 1998; Hille, 1977; Hondeghem, 1987; Hondeghem & Katzung, 1977), and its special case, the guarded receptor hypothesis, suggests the possibility compounds bind to a particular state only (Starmer & Courtney, 1986; Starmer et al., 1990, 1991). Both of these have been applied to computational (in silico) models of hERG binding (Gomis-Tena et al., 2020; Lee et al., 2017; Thurner et al., 2014; Veroli et al., 2013).

To capture all the possible consequences of state-dependent binding for a new compound within in silico models, all the above possibilities for drug binding to hERG should be considered. However, this raises the question of whether one size fits all—does the hERG binding model used in CiPA (Li et al., 2017) account for all the binding properties of interest, and do the model parameters reflect the underlying binding mechanisms? Furthermore, how sensitive is the proarrhythmic risk classification metric to any uncertainty in the binding mechanisms and also the underlying *physiological* hERG model (i.e., the description of channel gating in the absence of compounds)?

What is already known

- Compounds interact with the hERG channel with different state dependence and trapping properties.
- Proarrhythmic risk depends on the degree of trapping in the CiPA in silico modelling predictions.

What does this study add

- For many compounds, multiple binding mechanisms are consistent with data gathered under the CiPA guidance.
- Risk predictions are sensitive to these hERG binding mechanisms but more robust to gating model.

What is the clinical significance

- Clinical risk predictions for some compounds vary between plausible hERG binding mechanisms.
- Narrowing down plausible binding mechanisms will be needed to reduce this source of uncertainty.

In this study, we propose a method for considering a wide range of drug/ion channel binding models for hERG and rule out those that do not plausibly fit the available experimental data, resulting in an *ensemble of models* for each compound. The ensemble represents uncertainty in each compound's hERG binding mechanism. We then apply this method to the CiPA v1.0 validation study (Li et al., 2019) and examine how robust risk classifications are to this uncertainty in hERG binding mechanism. The same approach can be used whenever fitting drug binding data to ensure that we do not ignore this important source of uncertainty.

2 | METHODS

In this study, we designed a set of possible pharmacological binding models for the hERG channel that account for the known or postulated binding mechanisms (which we will describe in Sections 2.1 and 2.2). These models were calibrated to voltage-clamp electrophysiology data under the Milnes et al. (2010) protocol (Section 2.3.1) from Li et al. (2017, 2019), and plausible binding models that can explain the data well were selected (Section 2.3.2). We then used these binding models with different hERG physiological models to calculate the 'CiPA v1.0' risk metrics to assess the possible impact of different hERG binding mechanisms on such predictions (Section 2.4).

2.1 | hERG physiological models

The basic physiological models of hERG describe the drug-free control of voltage-dependent gating behaviour for the rapid delayed rectifier potassium current (I_{Kr}) at physiological temperature and conditions. Two physiological models are used in this study, with the transition rates following $p_i \exp(p_j V)$, where p_i and p_j are physiological model parameters taken from the literature. The first one, physiological model A, used in CiPA studies is shown in Figure 1a and is a six-state Markov model with two inactivated closed (IC) states, two closed (C) states, an inactivated (I) state, an open (O) state, and transition rates a_1 to a_7 and b_1 to b_7 (Dutta et al., 2017; Li et al., 2017). The second model, physiological model B, is a symmetric four-state model (Figure 1b) with transition rates k_1 to k_4, which is equivalent to a Hodgkin & Huxley-style model with one activation gate and one inactivation gate (the 37°C average model in Lei, Clerx, Beattie, et al., 2019; Lei, Clerx, Gavaghan, et al., 2019).

2.2 | Pharmacological binding models for hERG

To account for various known or proposed mechanisms for compounds binding to the hERG channel, a set of pharmacological binding models was designed as shown in Figure 2. The hERG physiological model is indicated in black, with common states I and O shown (on the right-hand side of each model from Figure 1), with dots representing the rest of either model.

In Figure 2, Model 1 represents a compound that can bind to both open (O) and inactivated (I) states, the drug is not trapped in the binding pocket, and the open and inactivated states share the same binding and unbinding rates (shown in the same colour). The binding rate is assumed to be proportional to the drug concentration $[D]$ raised to the power of a Hill coefficient, n, and the association rate constant is k_{on}; the unbinding rate is assumed to be a constant k_{off}. Model 2 allows binding only to the open state; the inactivated version of Model 2 (Model 2i) allows binding only in the inactivated state, using the guarded receptor hypothesis (Escobar et al., 2022; Lee et al., 2019). We have not observed any evidence that existing drugs bind at the resting potential ($\approx$80 mV) when the channel is closed, therefore we have excluded binding models that bind only to the closed state. Model 3 is a variant of Model 1 where transition between the compound-bound states are also allowed, and happen at the same rate as the (unbound) O $\rightleftharpoons$ I transitions.

Models 4 to 5i are the trapped equivalents of Models 1 to 2i, where the trapping component is indicated in grey, a 'mirror image' of the hERG physiological model with the same transition rates to admit the possibility of channels closing and preventing unbinding from CD or ICD states (not shown in the schematics) corresponding to C and IC in the drug bound channels. Model 6 relaxes the mirror trapping component of Model 4 by allowing an extra degree of freedom with a trapping rate factor k_{trap} multiplying the original transition rate. Models 7 to 10 allow an extra degree of freedom compared to Models 1, 3, 4, and 6 by assuming independent binding and unbinding rates for open and inactivated states—the modulated receptor hypothesis—whilst enforcing microscopic reversibility by specifying rates indicated by an asterisk as a function of the other rates in the closed loop (Colquhoun et al., 2004). Model 11 introduces independent trapped states for the open and inactivated compound-bound states with transition rates k_{trap} and k_{untrap}, which is inspired by a combination of the 'intermediate encounter complex' model in Windley et al. (2016) and the Li et al. (2017) model.

Model 12 is taken from Li et al. (2017). Here, rather than the drug binding rate being linearly proportional to $[D]^n$, instead it saturates, and this is represented using a Hill equation:

$$\text{Hill}([D]|\text{EC}_{50},n) = \frac{[D]^n}{[D]^n + \text{EC}_{50}^n}, \quad (1)$$

where EC_{50} is a half maximal effective concentration, that is, when $[D] = \text{EC}_{50}$, the binding rate is half of its maximum rate. Note that the binding rate parameter for Model 12 has a unit of ms^{-1}, so we denote it as $\hat{k}_{on}$ to differentiate it from k_{on} in the other binding models (which have units of $\text{ms}^{-1} \cdot \text{nM}^{-n}$). Model 12 is the same model (equations) as the CiPA v1.0 model proposed by Li et al. (2017)—the *reference model* for this study—but in Model 12 we will refit parameters. We also compare with the reference CiPA v1.0 parameters separately.

When $[D] \ll \text{EC}_{50}$, Model 12 reduces to the usual linear binding rate, $k_{on}[D]^n$; we consider this case separately as Model 13. Furthermore, Models 12 and 13 assume the untrapping rate follows a sigmoid function of the membrane voltage $X(V) = \left(1 + \exp\left((V_{1/2,\,trap} - V)/6.789\right)\right)^{-1}$ instead of the voltage dependence of the control condition which would involve a mirror image of the

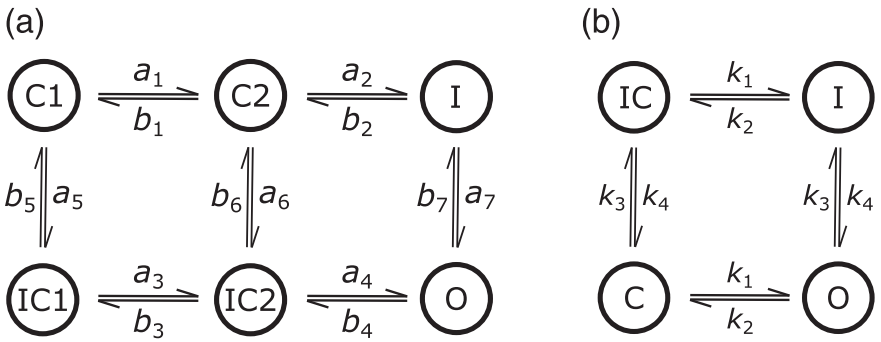

FIGURE 1 The base physiological models of the hERG channel considered in this study under drug-free conditions. (a) A six-state model from Li et al. (2017) and Dutta et al. (2017) with the states renamed to match their respective physical states. (b) A symmetric four-state model from Beattie et al. (2018) and Lei, Clerx, Beattie, et al. (2019). The models are used as the hERG model for studying drug effects.

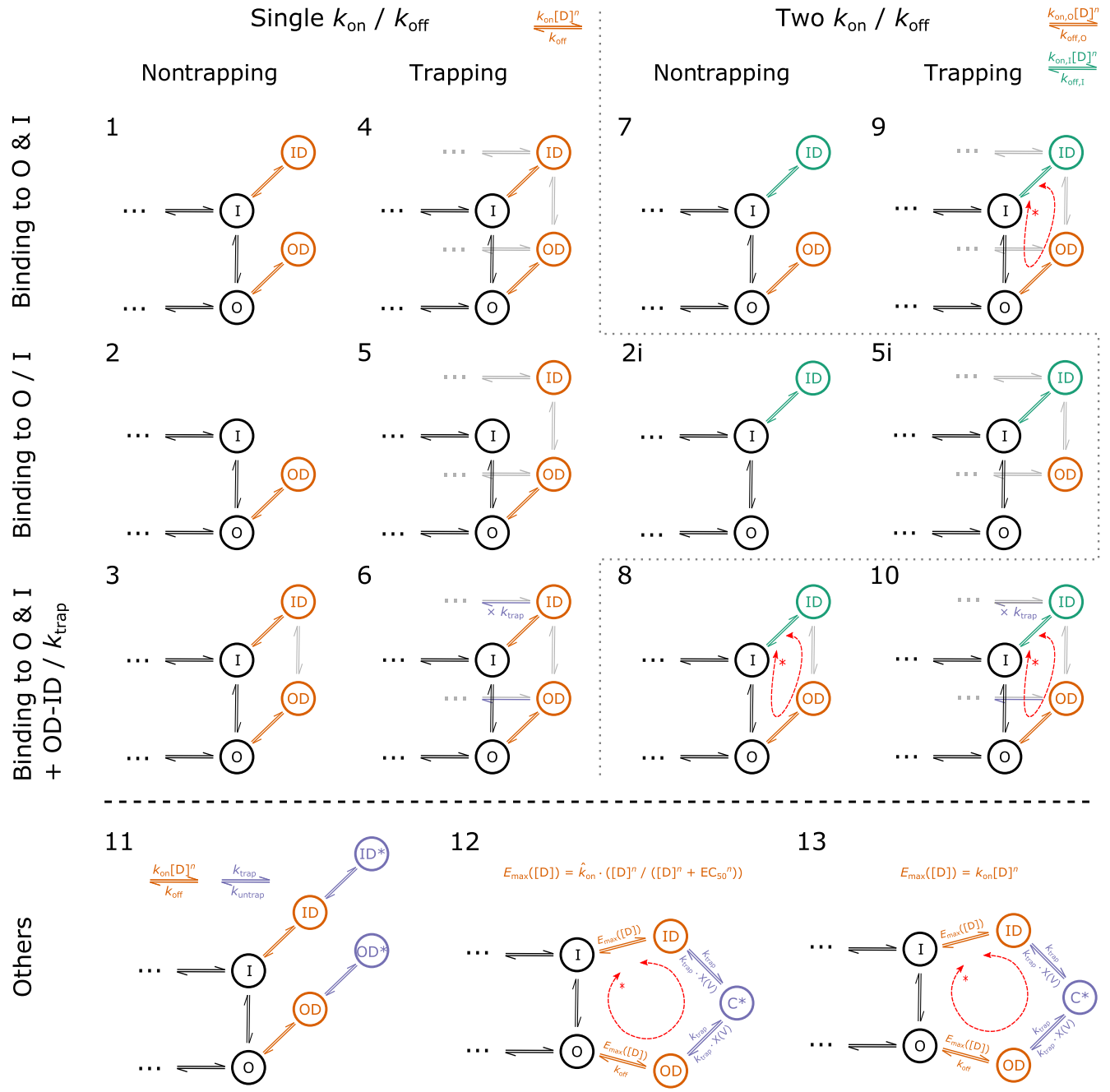

FIGURE 2 A set of pharmacological models representing different mechanisms of drug binding, where black (states I and O, and dots) is the physiological model of the hERG channel in Figure 1. Dashed double arrows indicate the rate marked with an asterisk is set by microscopic reversibility. Model 12 is identical to the pharmacological binding component in the CiPA v1.0 model.

hERG physiological model. Transition rates from ID→I are set by microscopic reversibility (indicated with an asterisk in Figure 2); they also assume a fixed trapping rate $k_{trap} = 3.5 \times 10^{-5}\,ms^{-1}$, with $V_{1/2,\,trap}$ altering the degree of trapping (Li et al., 2017).

We also included two additional models: Models 0α and 0β, as basic and standard 'conductance block' models for drug effects. We consider an 'all-state-blocker' model that has binding and unbinding rates, $k_{on}[D]^n$ and k_{off}, for all channel states. The degree of block is then independent of state occupancy and is equivalent to having a modulating fraction of unavailable channels or '*b* gate' such that we scale (multiply) the drug-free current by $(1-b)$. *b* itself follows the equation

$$\frac{db}{dt} = k_{on}[D]^n(1-b) - k_{off}b, \tag{2}$$

with an initial condition of $b = 0$ at the time a compound is first introduced, we call this Model 0β. Model 0α is a simpler conductance

scaling model which is derived by assuming Model 0β is an instantaneous process, that is, the degree of block b is set immediately to the steady state of Equation (2):

$$b_\infty = \frac{k_{on}[D]^n}{k_{on}[D]^n + k_{off}} = \frac{[D]^n}{[D]^n + k_{off}/k_{on}} = \frac{[D]^n}{[D]^n + IC_{50}^n}. \quad (3)$$

The ratio k_{off}/k_{on} in Model 0β is known as the dissociation constant and is equivalent to IC_{50}^n in the Hill equation in Model 0α. All the binding model parameters that need to be calibrated on a compound-specific basis are listed in Table 1.

2.3 | Data and statistical analysis

2.3.1 | Electrophysiology data

The voltage-clamp electrophysiology data were taken from the openly available 28 compound CiPA training and validation studies (Li et al., 2017, 2019) where manual patch-clamp experiments were performed on HEK293 cells (CLS Cat# 300192, RRID: CVCL_0045) stably expressing hERG1a subunit at 37°C—see Data Availability section. Data were originally collected using a modified Milnes' protocol (Milnes et al., 2010); the protocol had 10 sweeps measured with 10-ms time-point interval, and each repeat consisted of 1 s (with leak step) at the resting potential (−80 mV), followed by a long voltage step to 0 mV for 10 s, before returning to the resting potential for 14 s. For the details of the experiments, please refer to Li et al. (2017).

2.3.2 | Calibration of pharmacological binding models

We calibrated/fitted each of the pharmacological binding models in Figure 2 with each of the hERG physiological models in Figure 1 independently to the voltage-clamp electrophysiology data for each compound. The available data have been normalised to the control current, giving the *fraction of unblocked current*, which reveals the change in current due to the drug binding. Furthermore, only the data at the voltage step 0 mV (time interval 1.1–11 s) for the 10 sweeps were used; the remaining data at the resting potential (−80 mV) will have almost no current, giving little information about the drug binding. All models, except Model 0α, were calibrated by minimising the root-mean-square difference (RMSD) of the percentage current between the model output and the mean experimental data from 10 sweeps for four different concentrations of a compound, giving $4 \times 10 \times 990 = 39600$ data points for each compound. The optimisation was performed with logarithmic-transformed model parameters, except $V_{1/2,trap}$ in Models 12 and 13. This allows a better search across a wide parameter range, especially for the rate parameters. The optimisation was performed using the covariance matrix adaptation-evolution strategy (CMA-ES) algorithm (Hansen, 2006) in PINTS (Clerx et al., 2019) and was repeated 10 times from different initial guesses sampled from wide boundaries ($k_{on}, k_{off} \in [10^{-7}, 1]\,ms^{-1}$, $k_{trap}, k_{untrap} \in [10^{-9}, 10^{3}]\,ms^{-1}$, $\hat{k}_{on} \in [10^{-6}, 10^{9}]\,ms^{-1} \cdot nM^{-n}$, $EC_{50}^n \in [1, 10^{9}]\,nM^n$, $V_{1/2,trap} \in [0, 200]$ mV, and $n \in [0.2, 2]$) to ensure we arrived at a global minimum. The calibration was repeated for all 28 compounds listed in Li et al. (2019).

Model 0α is a special case of Model 0β where drug binding is approximated as instantaneously reaching steady state. Therefore Model 0α should not be calibrated to transient experimental data. Hence, the parameters of Model 0α were directly taken as the steady state of Model 0β—IC_{50}^n of Model 0α in Table 1 was calculated as the dissociation constant k_{off}/k_{on} of Model 0β, as Equation (3) suggests.

However, since each pharmacological binding model in Figure 2 was designed to model a specific mechanism, not all the models are expected to be able to describe all the compounds that were tested. Therefore each calibrated binding model was assessed by comparing its fitted RMSD to the RMSD of bootstrapped samples of the data which were computed as follows: since each of 10 repeated

TABLE 1 The model parameters for all the binding models in Figure 2. The asterisk indicates the rate parameter was determined by microscopic reversibility.

Model	Binding parameters					Trapping parameters	
0α	n	IC_{50}					
0β, 1, 3, 4	n	k_{on}	k_{off}				
2, 5	n	$k_{on,O}$	$k_{off,O}$				
2*i*, 5*i*	n	$k_{on,I}$	$k_{off,I}$				
6	n	k_{on}	k_{off}			k_{trap}	
7	n	$k_{on,O}$	$k_{off,O}$	$k_{on,I}$	$k_{off,I}$		
8, 9, 10	n	$k_{on,O}$	$k_{off,O}$	$k_{on,I}$	*		
11	n	k_{on}	k_{off}			k_{trap}	k_{untrap}
12	n	$\hat{k}_{on}$	k_{off}	EC_{50}		$V_{1/2,trap}$	
13	n	k_{on}	k_{off}			$V_{1/2,trap}$	

experiments at each concentration was independent, for one compound across all four concentrations, there are 10^4 permutations. We randomly selected (with replacement) one trace out of the ten available for each concentration to obtain a set of four traces for all concentrations; the RMSD of this set to the mean of the experimental data was computed, giving the RMSD of a 'bootstrapped' data trace. This process was repeated 1000 times to get a range of RMSDs based on these bootstrapped samples of the data. This essentially compares how well the models fit to the mean data relative to an individual data trace's fit to the mean data, providing a compound-dataset-specific measure of goodness-of-fit.

Although if the only source of error were normally distributed noise, we could compare the model fits against the standard error of mean, this would probably rule out all the models (including the CiPA v1.0 model). Therefore, a more relaxed threshold was chosen to allow for some degree of imperfection in our models of both binding mechanisms and noise processes/artefacts in the data, whilst still distinguishing between plausible and implausible binding mechanisms. A pharmacological binding model was classified as a *plausible model* if its RMSD was smaller than the maximum RMSD of the bootstrap samples of the data or *as plausible as the CiPA v1.0 model* if its RMSD was within 1.2× the RMSD of the reference model.

2.4 | AP models, q_{net}, and torsade metric scores

To assess the impact of the choice of hERG binding model on predictions of drug-induced proarrhythmic risk, we adapted the approach used in Li et al. (2019). We used the optimised CiPA v1.0 AP model by Dutta et al. (2017) for predicting the effects on AP due to different hERG binding mechanisms. The 'dynamic hERG-binding model' in the AP model was replaced with one of the successfully calibrated pharmacological binding models in Figure 2. To account for multiple ion channel block effects, the Hill equation characterised by the half-inhibition concentration (IC_{50}) and the Hill coefficient (n)—Model 0α—was used to model the drug effects on three other currents, the fast sodium current (I_{Na}), the late sodium current (I_{NaL}) and the L-type calcium current (I_{CaL}), using their reported median values.

The hERG physiological model can be either of the models shown in Figure 1. However, to use the new Figure 1b hERG physiological model in the CiPA v1.0 AP model, we recalibrated its I_{Kr} conductance, in control (drug-free) conditions, by matching the AP duration at 90% repolarisation (APD_{90}) at 0.5-Hz pacing (stimulus amplitude −80 A/F and 0.5-ms duration) at (quasi-)steady state after 1000 paces. We obtained a new I_{Kr} conductance of 0.0912 pA/pF for the hERG physiological model B in the AP model that resulted in the same APD_{90} as the CiPA v1.0 model.

The hERG-binding-model-replaced-AP models were then used to calculate the q_{net} metric and the proarrhythmic risk prediction. For each model and compound, pacing at 0.5 Hz was initialised from the steady state under control-conditions and continued for 1000 paces after compound addition, at multiples of each compound's maximum therapeutic concentrations (C_{max}). The q_{net} metric was defined as the net charge over one beat carried by I_{Kr}, I_{NaL}, I_{CaL}, the transient outward potassium current (I_{to}), the slow rectifier potassium current (I_{Ks}), and the inwardly rectifying potassium current (I_{K1}); this was computed by integrating the sum of the six currents between two consecutive stimuli (with time step 0.01 ms) using the trapezium rule. The proarrhythmic risk prediction was made using the *torsade metric score*, defined as the mean q_{net} value averaged at $1\times, 2\times, 3\times, 4\times C_{max}$.

Finally, an ordinal logistic regression model (all-threshold variant, Rennie & Srebro, 2005) was used to estimate the new drug-induced proarrhythmic risk thresholds for low-, intermediate-, and high-risk categories, using the torsade metric as the feature. The classifier was trained with L2 regularisation using only the training compounds and was solved with the L-BFGS-B algorithm in SciPy (Virtanen et al., 2020). The two thresholds for separating (a) the low-risk category from intermediate/high and (b) high from low/intermediate risks were calculated using

$$\text{Threshold } 1 = \frac{1}{\beta_1}\log\left(e^{-\beta_0^b} - 2e^{-\beta_0^a}\right), \tag{4}$$

$$\text{Threshold } 2 = \frac{1}{\beta_1}\log\left(\frac{e^{-\beta_0^a-\beta_0^b}}{e^{-\beta_0^b} - 2e^{-\beta_0^a}}\right), \tag{5}$$

where β_0^a and β_0^b are the intercepts, and β_1 the linear coefficient (of the torsade metric), of the linear equations that map the torsade metric through a logistic function to the cumulative probabilities of the risk categories within the logistic regression model. Because the action potential shape changes slightly with a different physiological hERG model, then q_{net} at control and derived thresholds also change. The metric values for each physiological model were normalised using

$$\text{Normalised } x_m = \frac{x_m - \text{Threshold } 2_m}{\text{Threshold } 1_m - \text{Threshold } 2_m}, \tag{6}$$

where x can be either q_{net} or the torsade metric score, and m denotes the physiological model (either model A or B), such that the boundary between high-risk and intermediate/low is at 0 and between low-risk and high/intermediate is at 1 to facilitate comparison of classification between physiological models.

2.5 | Nomenclature of targets and ligands

Key protein targets and ligands in this article are hyperlinked to corresponding entries in https://www.guidetopharmacology.org, and are permanently archived in the Concise Guide to PHARMACOLOGY 2021/22 (Alexander et al., 2021).

3 | RESULTS

3.1 | Multiple binding mechanisms can explain the same drug effects

All binding models (Figure 2) were calibrated to the experimental data for each compound independently and compared against the maximum RMSD for bootstrapped samples of the data. Figure 3 shows the calibrated binding models (left) and their RMSDs to the mean experimental data (right) across all binding models, for three example compounds: dofetilide (top), **terfenadine** (middle), and verapamil (bottom). The percentage current plots in Figure 3 (left) show *only* the effect of the drug over time for the 10 pulses of holding potential (0 mV) in the CiPA-Milnes protocol. Regardless of the physiological models (A, squares and B, circles), the results of the calibration of the binding models were similar. The results of all the remaining compounds are shown in the Supporting Information.

For dofetilide, a trapped drug (Milnes et al., 2010), *all* binding models except the steady-state conductance scaling model (Model 0α) were able to fit the calibration data, and so we cannot unpick the binding mechanisms of this drug with these data. The four grey horizontal lines in Figure 3 (left) are predictions of Model 0α, the only implausible model for dofetilide. Model 0α was the only model that showed no dynamics in the percentage current plots as, by definition, it scales only the conductance of the model so its effect on I_{Kr} must be constant over time. Another model that lacked in the drug dynamics was Model 0β, the all-state binding model, which marginally passed the RMSD check. Model 0β modelled the drug effect with the b gate in Equation (2) that is independent of channel state/voltage, producing a single exponential decay over time—even during the long resting potential (−80 mV) of CiPA-

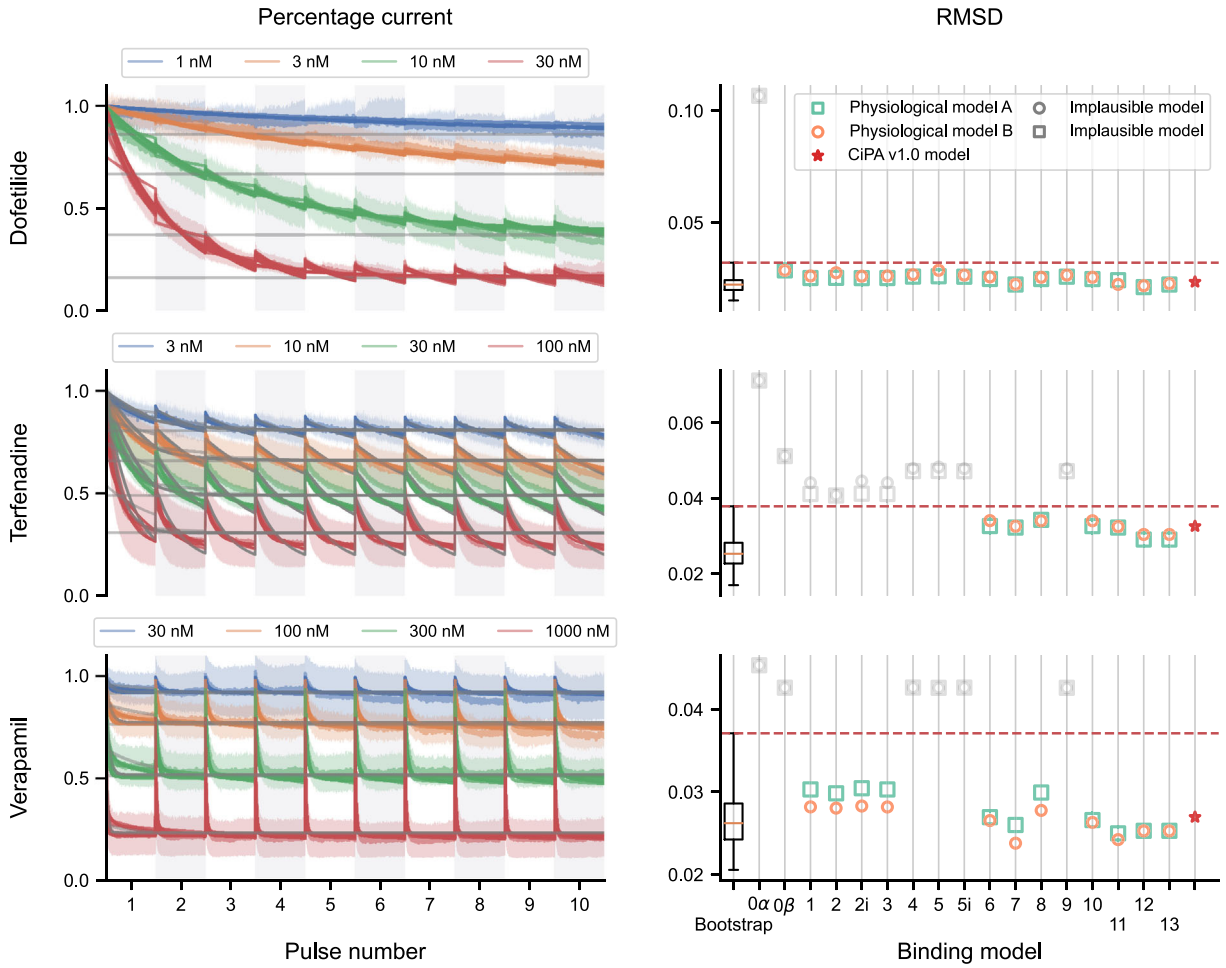

FIGURE 3 Calibration of the binding models and their RMSDs for three example compounds: dofetilide (top row), terfenadine (middle row), and verapamil (bottom row). The left column shows the percentage current of the data (semitransparent line for the mean and highly-transparent area showing ± one standard deviation) and the calibrated binding models (solid, smooth lines) for all four concentrations used during calibration. The right column shows the RMSD of all models compared to the RMSD of the bootstrap samples of the data (box-plot) and the reference model, CiPA v1.0 (red star). Both physiological models A (green squares) and B (orange circles) are shown for comparison. The horizontal red dashed line indicates the maximum RMSD of bootstrapped samples of the data. Grey lines/markers on each panel are the binding models that are ruled out through the RMSD comparison (above the red dashed line)—implausible models.

Milnes protocol (although not shown) when the channels were in the closed state(s), resulting in the drop in current between pulses, when the data show (if anything) a slight restoration of current between pulses.

The other two example compounds in Figure 3, terfenadine and verapamil, had a weaker to no trapping tendency compared to dofetilide; that is, current recovers significantly between 0 m V pulses, suggesting unbinding rather than trapping at −80 mV. Interestingly, more binding models failed to fit to the experimental data of these two drugs. For terfenadine, a weakly trapped drug (Kamiya et al., 2008; Stork et al., 2007; T. Yang et al., 1995) with slow binding rates (Li et al., 2017), only Models 7 and 8 (variants of the independent open and inactivated binding model) and Models 6 and 10–13 (variants of *flexible*-trapping models) were able to explain its drug effect as well as the bootstrap samples of the data, although a few more non-trapping models were merely marginally ruled out. For verapamil, a nontrapped drug (S. Zhang et al., 1999), our approach successfully disqualified *all simple*-trapping models (Models 4, 5, 5i, and 9), as well as the conductance blocking and the all-state binding models (Models 0α and 0β). However, it left the non-trapping models (Models 1–3, 7, and 8) and the flexible-trapping models (Models 6 and 10–13) as plausible candidates for the binding mechanism.

Figure 4 presents a summary of the binding models with physiological model A, which gave plausible fits to the experimental data and/or performed similarly to the CiPA v1.0 model (shown in light/dark greens and both are considered as plausible models in subsequent analyses); a summary for those with physiological model B are provided in the Supporting Information; the results were very similar with only minor differences for cisapride, **ibutilide**, and **loratadine**. We observed no obvious pattern between the proarrhythmic risk of drugs and the type of binding models ruled implausible. A few more nontrapped drugs were identified simply based on the ruling out of the simple-trapping models (Models 4, 5, 5i, and 9) as in the case of verapamil (Figure 3), such as cisapride (Milnes et al., 2010) and **droperidol** (Stork et al., 2007; Windisch et al., 2011). For most of the drugs, multiple binding models were able to explain the observed drug effects using the experimental data collected through CiPA-Milnes protocol.

3.2 | Inferred binding rates can be strongly dependent on binding mechanism

Studying drug binding kinetics, such as the binding and unbinding rates, is important for understanding the drug effects on the channels and predicting behaviour in new situations. Figure 5 shows inferred binding rate parameters k_{on}, unbinding rates k_{off}, and the Hill coefficients n of the calibrated binding models. All binding models have k_{on}, k_{off}, and n, apart from the conductance scaling model (Model 0α) which has only two parameters IC_{50} and n (Table 1). Models 7–10 have independent binding rates for the open and inactivated states, giving two k_{on} shown as empty (for open) and filled (for inactivated) markers; only Model 7 has two (free) k_{off}, shown in the same way, as Models 8–10 have closed-loop states which reduce one degree of freedom due to microscopic reversibility (Figure 2). The CiPA v1.0 model is shown as red stars; the two physiological models, A and B, are shown together as squares and circles, respectively, and the observed results remained similar regardless of the physiological model. The results for all the remaining compounds are shown in the Supporting Information.

Taking verapamil as an example, the inferred binding rate parameter k_{on} was similar for most of the successfully calibrated binding models (Figure 3). The two binding rate parameters $k_{on,O}$ (empty marker) and $k_{on,I}$ (filled marker) for the plausible models—Models 7, 8, and 10—were similar too, and their average roughly equalled k_{on} of the other models. The similarity suggested that the independence assumption may be superfluous in this case, because if the two inferred rates were the same, the models would be equivalent to those without the extra degree(s) of freedom (Models 1, 3, and 6). Similarly, the unbinding rates k_{off} were similar for all binding models, except the $k_{off,O}$ (empty marker) and $k_{off,I}$ (filled marker) in Model 6; all of the inferred Hill coefficients n were within the range of 1.3–1.8. It is worth noting that the k_{off} of Model 12 and the CiPA v1.0 model (the same binding model structure but under different calibration schemes) shared similar inferred values for verapamil but their $\hat{k}_{on}$ were not shown due to different units.

For metoprolol, the inferred k_{on} were heavily binding-model-dependent, with a coefficient of variation (defined as the ratio of the standard deviation to the mean, for the plausible models) of 607%, as compared to 141% for verapamil. The other two parameters k_{off} and n were similar across the calibrated binding models. Unlike verapamil, the inferred k_{off} of Model 12 and the CiPA v1.0 model were inconsistent, using the same set of experimental data but with different calibration schemes; see also **mexiletine** in the Supporting Information. The differences in the inferred parameters may raise questions about the calibration data and the complexity of the model structure used, leading to potential parameter unidentifiability issues (Whittaker et al., 2020; see also Section 4).

3.3 | q_{net} with different binding mechanisms can diverge

Thus far, we compared the binding models of hERG when calibrated to voltage-clamp experimental data for various compounds. Here, we show the results of our investigation on the impacts of these binding models on APs and risk simulations (Section 2.4), whilst accounting for multichannel effects, following Li et al. (2019). Figure 6 shows the metric q_{net} at various C_{max} levels for all binding models, with implausible models shown with dotted lines. The torsade metric decision boundaries for the low-risk (green), intermediate-risk (blue) and high-risk (red) categories in Li et al. (2019) (0.0689C/F and 0.0579C/F, respectively) are indicated as dashed horizontal lines for reference. Various degrees of q_{net} spread were observed across the binding models for different compounds.

For example, diltiazem is a strong I_{CaL} blocker relative to its I_{Kr} effects, therefore the drug effect on APs measured through q_{net}

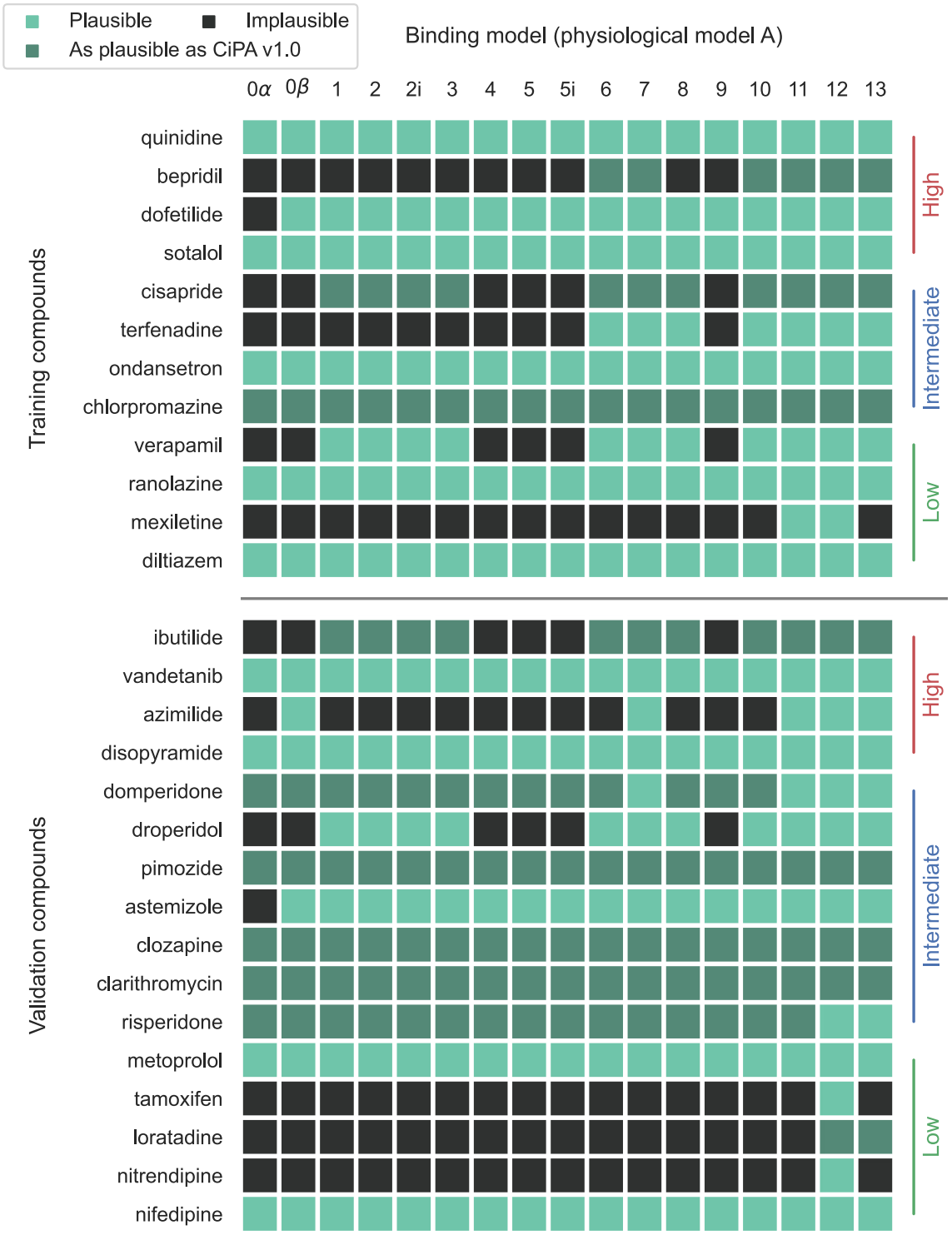

FIGURE 4 Summary of the selected binding models with physiological model A for all compounds. A binding model (column) is considered to be appropriate for a compound (row)—a plausible model—if coloured in green, where the RMSD of the model to the averaged data is either smaller than the RMSD of the bootstrap samples of data or similar to the CiPA v1.0 model to the averaged data; it also shows the models that are as plausible as the CiPA v1.0 model (darker green) but worse than the bootstrap samples of data. Model 12 is identical to the pharmacological binding component in the CiPA v1.0 model. Compounds are sorted according to the training and validation lists, and their proarrhythmic risks.

reflects mostly the drug block of I_{CaL} and the effects of different I_{Kr} binding models are insignificant. Nifedipine and verapamil are also multi-channel blockers of I_{CaL} and I_{Kr}, with similar block levels for each current. However, the uncertainty in their resulting q_{net} predictions were drastically different—nifedipine showed tight q_{net} predictions across the binding models, whilst verapamil produced a wide spread.

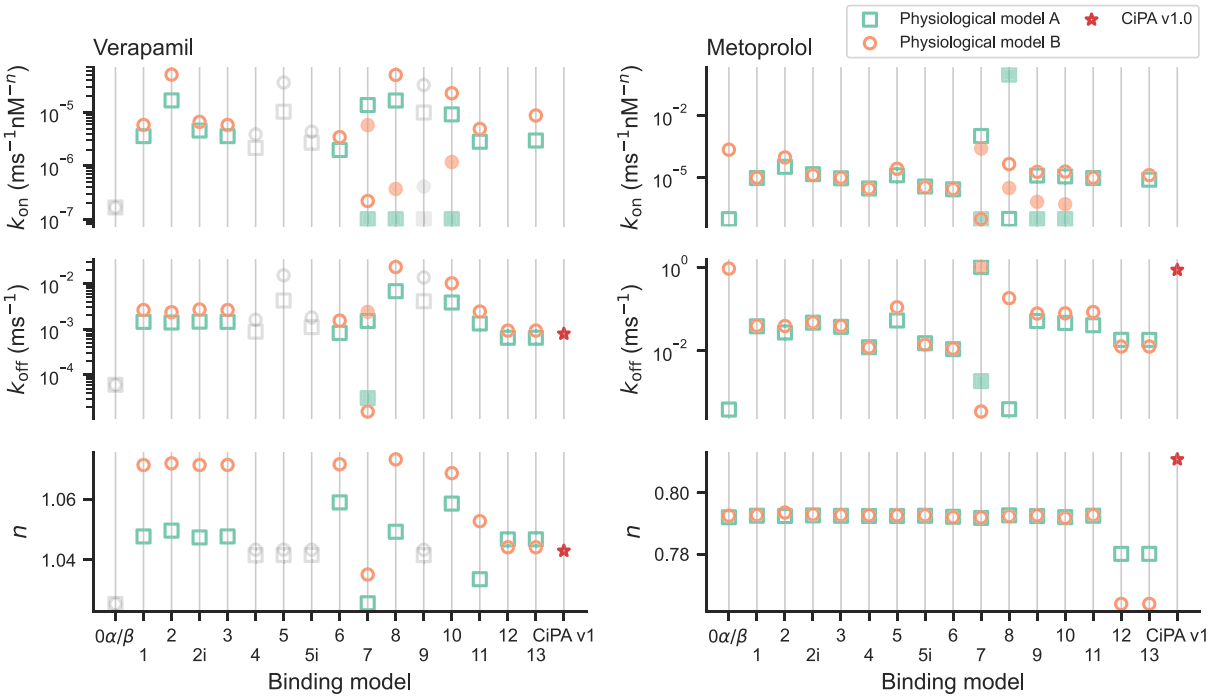

FIGURE 5 Binding rate parameters k_{on} (top row), unbinding rates k_{off} (**middle row**), and the Hill coefficients n (bottom row) of the calibrated binding models for two example compounds: verapamil (left column) and metoprolol (right column). Both physiological models A (green squares) and B (orange circles) are shown for comparison. Models 7–9 have independent binding and unbinding rates for open and inactivated states; filled squares/circles are the rates for the inactivated states. The models in grey are implausible models. Model 12 is identical to the pharmacological binding component in the CiPA v1.0 model (red star). $\hat{k}_{on}$ is not shown for Model 12 and CiPA v1 due to different units.

Figure 6 (bottom row) also shows three more examples: dofetilide, cisapride, and bepridil. These compounds are almost pure I_{Kr} channel blockers at these concentrations. Again, they showed inconsistent spread of q_{net} predictions from the *plausible* binding models, demonstrating the importance of identifying the correct binding mechanisms or at least narrowing down the possibilities.

Furthermore, in general, we also observed an increasing spread of the q_{net} predictions from plausible binding models at higher C_{max} levels; verapamil is one of the most obvious examples. This phenomenon showed the differences between the binding mechanisms were amplified with higher concentrations of the drug, and at the top concentrations verapamil spanned all risk categories. However, the torsade metric uses only 1–4× C_{max} of q_{net}—the metric that was used to train the classification model (ordinal logistic regression model) for producing the decision boundaries of the risk categories, and we examine risk predictions in this range in the next section.

3.4 | Binding mechanisms can result in substantial uncertainty in torsade risk

Figure 7 (left) shows the torsade metric predictions of all binding models with physiological model A for all compounds. The drugs are sorted according to their proarrhythmic risk categories and are split into training and validation lists (Li et al., 2019); the same decision boundaries as Figure 6 are shown as dashed vertical lines, for the low-risk (green), intermediate-risk (blue), and high-risk (red) categories.

The torsade metric predictions for the same compound resulted in a large variation—indicating high uncertainty in the proarrhythmic risk prediction—due to different binding mechanisms. However, it is worth emphasising that these plausible binding models were able to explain the observed experimental data of the compounds either better than the bootstrap samples of the data or as well as the CiPA v1.0 model, therefore the acquired experimental data were not able to resolve the resulting uncertainty. The reference model, CiPA v1.0, is shown as circles, and the conductance scaling model, Model 0α, is shown as squares; unexpectedly, Model 0α, which had the worst performance during the calibration process (Figure 4) and was ruled out in most cases, did not cause any obvious outlying torsade metric prediction (cf. the extreme RMSD values of Model 0α in Figure 3), and in fact it was usually not the one giving the predictions at the extremes, showing the nonlinearity in the relationship between the calibration and the torsade metric prediction. Also, interestingly, the degree of variation tended to be larger for drugs in higher proarrhythmic risk categories, for both training and validation drugs, perhaps because hERG block was more dramatic in these compounds (see Section 4).

The corresponding AP predictions for some of the drugs at 4× C_{max} are shown in Figure 7 (right). In general, as expected, a strong AP prolongation—longer AP duration—correlated with a high torsade metric risk category: the shortest AP duration for the low-risk category in green, followed by intermediate in blue, and then the longest

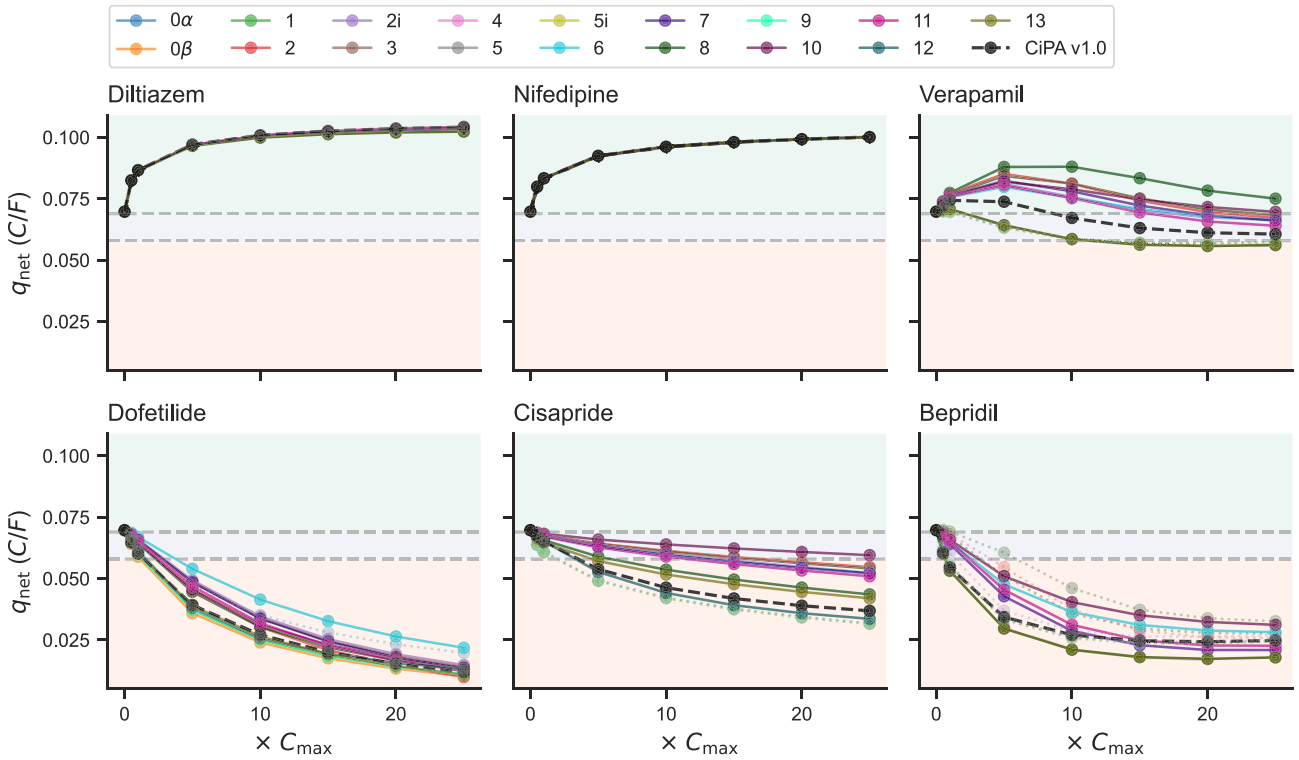

FIGURE 6 q_{net}, the net charge carried by currents active in plateau and repolarisation over one beat of AP (I_{Kr}, I_{NaL}, I_{CaL}, I_{to}, I_{Ks}, and I_{K1}) at various multiples of C_{max} for all binding models with six example drugs. Here, diltiazem, nifedipine, verapamil, dofetilide, cisapride, and bepridil are shown, revealing a spectrum of behaviours from the binding models. Dashed horizontal lines indicate the decision boundaries for the low-risk (green), intermediate-risk (blue), and high-risk (red) categories for the torsade metric score (average q_{net} at 1–4× C_{max}) in Li et al. (2019). The implausible models are shown as transparent dotted lines, and the CiPA v1.0 model is shown as black dashed lines.

AP for high risk in red. The plausible binding models can result in metric predictions with high uncertainty, even spanning multiple risk categories; for example, domperidone predictions span all three risk categories.

3.5 | The effect of hERG physiological model on risk classification is subtle

Finally, we compared the effects of the choice of the I_{Kr} physiological model (Figure 1) in predicting the torsade risk classes. The 'O'Hara-Rudy CiPA v1.0' model (Dutta et al., 2017) had hERG physiological model A replaced with physiological model B (solid lines; Lei, Clerx, Beattie, et al., 2019; Lei, Clerx, Gavaghan, et al., 2019), the I_{Kr} maximum conductance was re-calibrated to match the APD_{90} of the CiPA v1.0 AP model (dashed lines), as shown in Figure 8a (blue lines). The I_{Kr} within the two AP models, shown as orange lines, reveals differences in the dynamics of the two hERG physiological models. Although the total charge carried by the two I_{Kr} models is similar (0.190C/F and 0.144C/F for models A and B, respectively), physiological model B has a smaller current during the early phase of the AP—depolarisation to plateau—and plays a more important role during repolarisation. The two I_{Kr} physiological models show a similar overall transition between the states (Figure 8a): starting from mainly the closed state(s) to the inactivated state(s) during depolarisation/plateau before occupying the open state and back to the closed state(s).

For physiological model B, training the ordinal logistic classification model to the torsade metric of the training drugs for all the *plausible* binding models adjusted the risk category thresholds to be 0.0584C/F and 0.0483C/F for separating the low-risk category from intermediate/high and the high-risk category from intermediate/low, respectively; the fitted ordinal logistic classifier parameters are provided in Table S1. The shift in the boundaries was consistent with the change in the net charge carried by physiological model B (and alteration to AP shape, which also affects other currents), which resulted in a new control value of q_{net}. The two new decision boundaries are used for physiological model B in Figure 8b,c.

In Figure 8b,c, to compare the differences in the metric predictions between the two physiological models, the metrics predicted by each model were normalised to its decision boundaries using Equation (6), such that the normalised decision boundaries are 0 and 1 for both models; the results for only physiological model B (without normalisation) are shown in Figure S25. Replacing the physiological model of I_{Kr} still produced a similar trend for the drug risk categories, although some of the drugs, such as bepridil and **tamoxifen**, were clustered closer to the new decision boundaries. The observed differences could result from the new I_{Kr} model, the choice of calibration protocol, and the choice of the metric, all of which were designed for CiPA v1.0.

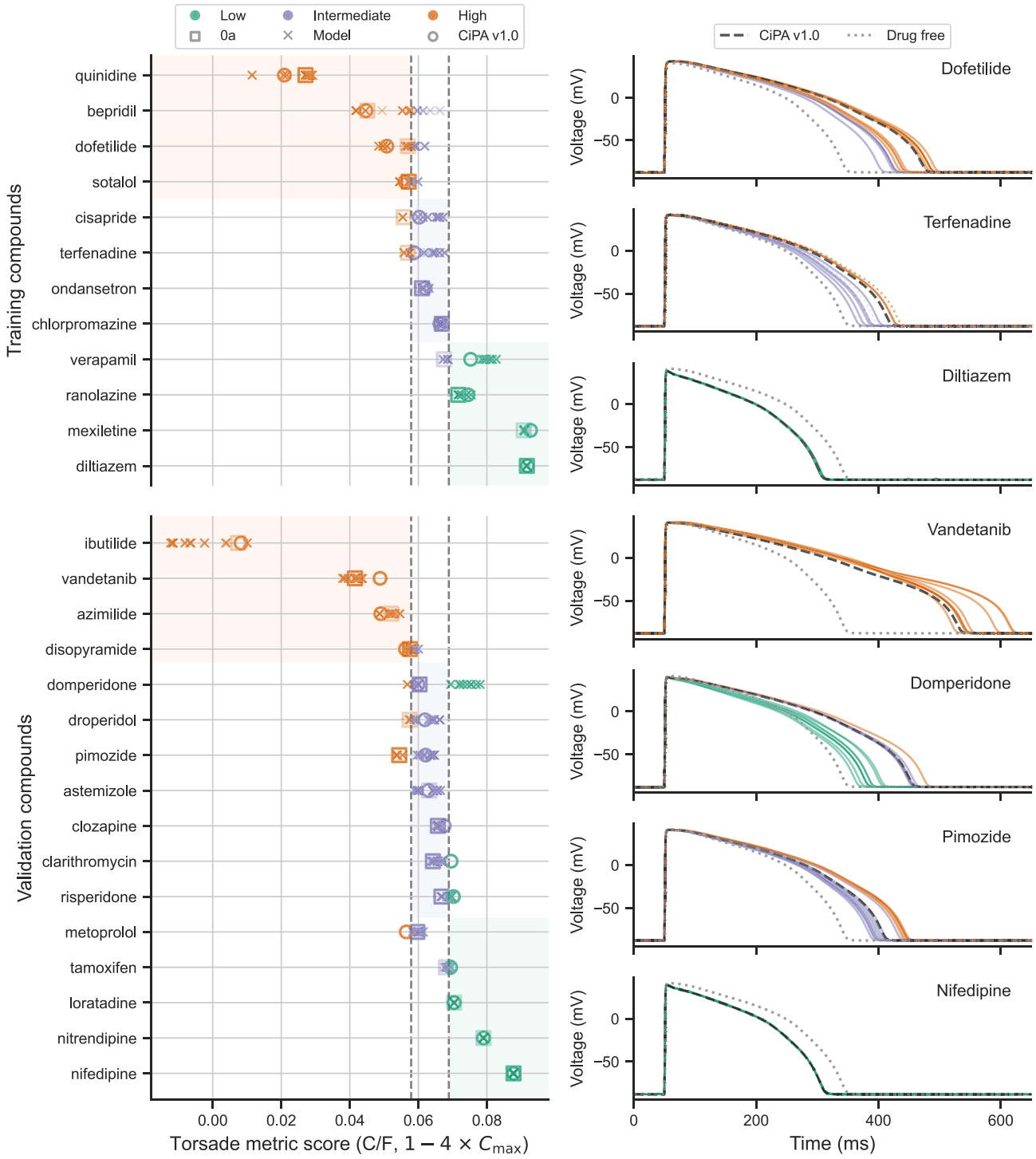

FIGURE 7 The torsade metric predictions, the mean q_{net} of 1–4× C_{max}, of all binding models with physiological model A for all compounds, and the corresponding AP predictions for seven example drugs. (Left) Drugs are sorted according to their proarrhythmic risk categories. Dashed vertical lines indicate the CiPA v1.0 decision boundaries for the low-risk (green), intermediate-risk (blue), and high-risk (red) categories. The CiPA v1.0 model is shown as circles, and the conductance scaling model, Model 0α, is shown as squares. (Right) The AP predictions of dofetilide, terfenadine, diltiazem, vandetanib, domperidone, pimozide, and nifedipine at 4× C_{max} are shown, revealing a range of different behaviours from the binding models, indicated with the same colour code as shown on the left. The plausible models are shown as coloured solid lines, the implausible models as transparent dotted lines, and the CiPA v1.0 model as black dashed lines. The drug-free (control conditions) model is shown as grey dotted lines.

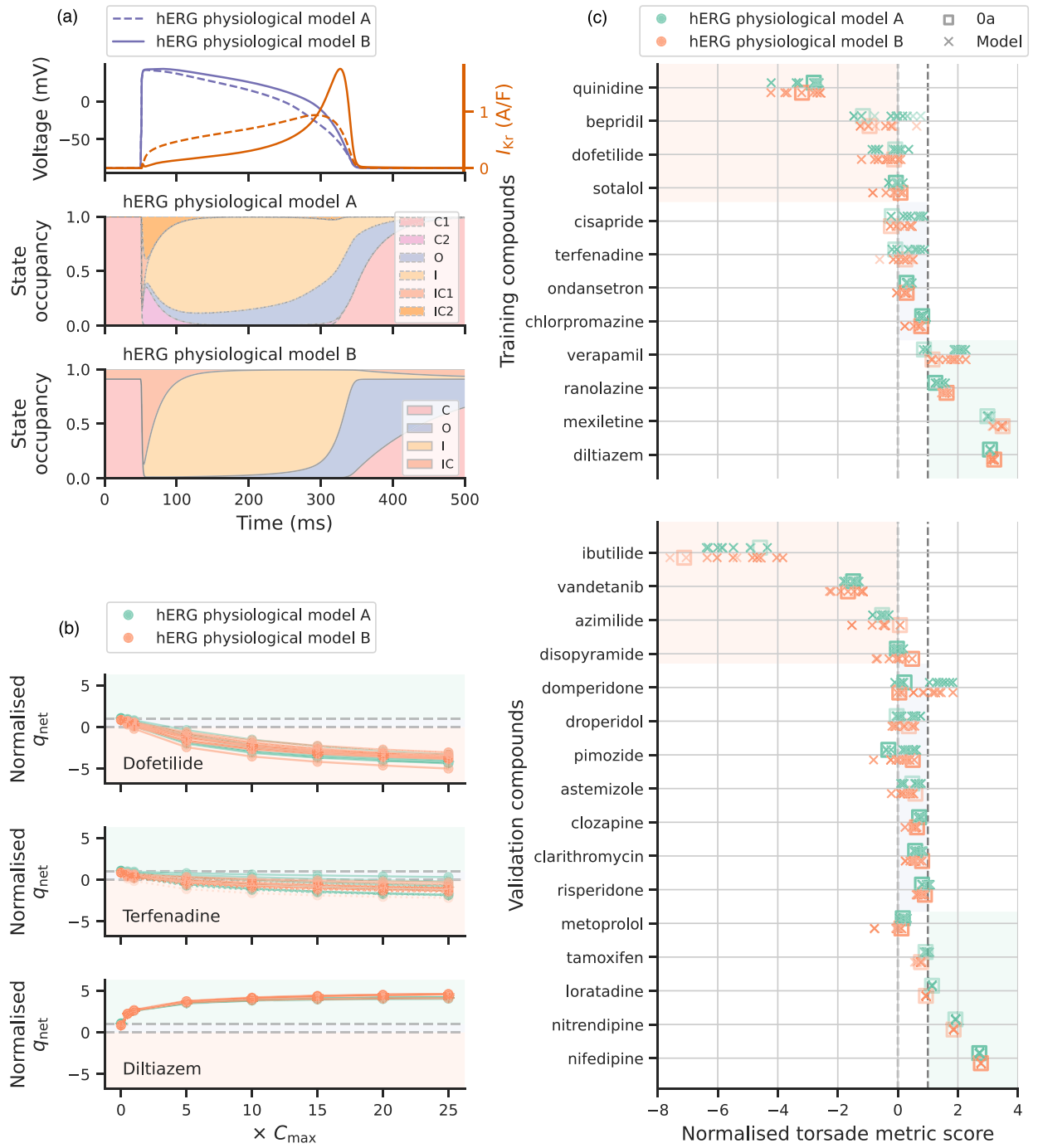

FIGURE 8 Comparisons of hERG physiological model B in predicting the q_{net} metric and the torsade metric with hERG physiological model A. (a) Comparison of AP, I_{Kr}, and state occupancy using the two hERG physiological models A (dashed lines) and B (solid lines). (b) Normalised q_{net} metric at different C_{max} levels for all binding models with physiological models A (green) and B (orange) for one example of each risk category prediction: dofetilide, terfenadine, and diltiazem. More compounds are shown in the Supporting Information. (c) Normalised torsade metric predictions of all binding models with physiological models A (green) and B (orange) for all compounds. Dashed vertical/horizontal lines indicate the normalised decision boundaries for the low-risk (green), intermediate-risk (blue), and high-risk (red) categories.

4 | DISCUSSION

In this study, we have designed a set of pharmacological binding models for the hERG channel. After selecting a subset of plausible binding models through calibration to the voltage-clamp electrophysiology data under CiPA-Milnes protocol, we compared their effects, as well as the effects of having different physiological hERG models, on proarrhythmic risk predictions.

Our pharmacological hERG binding models accounted for most of the plausible mechanisms by which a compound might bind to the

hERG channel. The choice of these models has covered many of the literature binding models of hERG. For example, our simple binding models (Models 2, 2i, and 7) and trapping models (Models 5, 5i, and 9) are similar to models referred to as 'unstuck' and 'stuck', respectively, in Gomis-Tena et al. (2020); Escobar et al. (2022). Models 0α, 7 and 11 were used in Windley et al. (2016) to study the effects of compounds such as cisapride.

In Figures 3 and 4, we demonstrated that our approach can be used to distinguish some of the simpler binding mechanisms based on the CiPA-Milnes protocol data for some compounds, such as terfenadine and verapamil; resulting in plausible binding mechanisms consistent with the literature. It was also able to highlight certain similarities between some compounds such as bepridil (Kamiya et al., 2006; Pareja et al., 2013) and terfenadine (Stork et al., 2007) where only flexible-trapping models were deemed plausible to explain the observed data; indeed, studies with specifically designed voltage protocols consider these two compounds to be trapped slow-binders (Kamiya et al., 2008). Also, our approach was able to highlight compounds, such as tamoxifen, loratadine, and **nitrendipine**, where none of the models (not even the CiPA 1.0 model) were able to fit the data satisfactorily. On closer inspection (Supporting Information) the data of loratadine, and nitrendipine showed a slight *increase* of the (percentage) current over time during the 0 m V pulses, raising potential data quality issues (Lei, Clerx, et al., 2020; Montnach et al., 2021; Raba, et al., 2013) or the need for methods to account for inadequacy of the models (Lei, Ghosh, et al., 2020; Lei & Mirams, 2021) and/or new (un)binding mechanisms to explain this observation; whilst for tamoxifen, there was a more obvious data quality issue for one of the concentrations. In Figure S26, we also included the results of fitting all the binding models whilst assuming the Hill coefficient (number of binding sites) to be $n = 1$. However, in this case, most of the binding models failed to fit to many of the compounds—being classified as implausible models—suggesting the importance of the extra degree of freedom provided by the Hill coefficient in explaining these observations, although we do not eliminate the possibility of this having been caused by some experimental artefact resulting in a drift/rundown that the analysis approach mistakes for non-saturating or more quickly/slowly saturating hERG block.

It may be better to think of our 'plausible' binding models as 'not implausible', there is no evidence that any individual model is correct, indeed by their nature some contradict others, it is just that they cannot be ruled out yet based on the available data. It is desirable for the calibration data to contain enough information to rule out as many binding models as possible, in an ideal world leaving just a single plausible model. But with the resulting ensemble at present, we can objectively and quantitatively describe a compound's binding mechanism instead of qualitatively classifying the compound as 'trapped', 'binding to open state', and so forth. However, we observed that the data elicited under the CiPA-Milnes protocol, which was originally designed to differentiate between trapped and nontrapped compounds (Milnes et al., 2010), were *not* able to distinguish between all the possible binding mechanisms, or indeed even whether trapping occurs, for all compounds (Figure 3). This suggests the need for designing better, richer experimental protocols for model calibration and selection (Lei et al., 2023), for instance gathering data on block onset at different voltages (Gomis-Tena et al., 2020; Lee et al., 2019), and to overcome some of the difficulties in measuring fast time-courses of block (Windley et al., 2017). Indeed a range of protocols may needed for assessing fast- and slow-binding compounds that bind via multiple mechanisms.

The model structure is not only useful for identifying the binding mechanisms; the inferred model parameters, such as binding/unbinding rates, for the *plausible* pharmacological binding model(s) can be used as a proxy to quantitatively assess the binding behaviour and dynamics. However, we showed that, with the limitations of the calibration data, not all plausible models recover the same binding and unbinding rates, although their ratios, the dissociation constants k_{off}/k_{on} of the models, were more consistent (Figure 5 and Supporting Information). This leads to a more complicated interpretation of the binding properties. Without being able to identify the correct binding mechanism(s), we would not be able to study the true binding/unbinding rates of the compound. Moreover, for more complex pharmacological models, the inferred parameters may even be subject to the calibration scheme and procedure: For example, the inferred unbinding rate k_{off} of Model 12 and CiPA v1.0 were inconsistent (Figure 5), although our Model 12 gives lower RMSDs (Supporting Information). The different optimal parameters in CiPA v1.0 versus Model 12 fits could be due to the use of a different objective function—there a tailored weighted sum of squares of residuals, and based on fewer optimisation runs which could perhaps make local rather than global optima more likely (Li et al., 2017). We note that this is not the same as the unidentifiability issue between, in our notation, $\hat{k}_{on}$ and EC_{50} discussed in Li et al. (2019), suggesting this is a difficult optimisation problem. Our findings emphasise the need for careful design of experiments when parameterising complex models (Whittaker et al., 2020).

In Figure 4, we observed that constant instant conductance block (Model 0α) was not classified as a plausible model for most of the compounds, as we would expect, the goodness of fits were inadequate and poor (Figure 3). Yet, the torsade metric predictions by Model 0α were not dissimilar to the other models (Figure 7; see also Han et al., 2019; Mistry, 2019), which was likely due to the difference between using transient data (Milnes' protocol) and predicting steady-state (q_{net}/torsade metric) conditions (Farm et al., 2023). However, we believe the torsade metric predictions of Model 0α were acceptable only because of the steady-state nature of the metric. If Model 0α were to be used to predict transient APs under certain changes of conditions or pacing rates, then kinetic effects would be neglected and bad predictions would likely result.

In Figure 7, we also noticed that the degree of variation tended to be larger for drugs in higher proarrhythmic risk categories. This phenomenon was thought to be due to the multichannel effects, which either compensate for the effects of different hERG binding mechanisms or make them insignificant. However, if our multiple-binding-model approach was applied to other types of current, such as I_{CaL}, it may result in a similar level of uncertainty in their binding mechanisms, leading (correctly) to a higher level of uncertainty in the

risk predictions than we observed (Figure 7), particularly for compounds that mainly block I_{CaL} (e.g., diltiazem and nifedipine). Nonetheless, such an observation also implies that it is likely to be most important to determine the correct hERG binding mechanism when predicting drugs with higher proarrhythmic risk. Also, given some of the risk prediction spanned multiple risk categories, we advocate efforts to reduce the uncertainty in binding model. Overall, the results highlight the importance of the details of hERG binding mechanisms.

Furthermore, we have studied the effects of two different hERG physiological channel gating models (Figure 1) on proarrhythmic risk predictions. The CiPA v1.0 model uses hERG physiological model A (Li et al., 2017), which was designed to closely match the I_{Kr} in O'Hara et al. (2011) which itself was fitted to the native I_{Kr} of a cardiac myocyte—composed of a mixture of hERG1a/1b channels or hetero-tetramers (Jones et al., 2004; Sale et al., 2008) and any associated (possibly still unknown) subunits and regulatory components, rather than just hERG1a. In contrast, physiological model B was trained using data from a cell line over-expressing hERG1a (Lei, Clerx, Beattie, et al., 2019), which explains why the two models exhibit marked differences in their predicted kinetics (Figure 8A). Since the drug-binding calibration data were also gathered using hERG1a cell lines, we might expect that physiological model B could capture the drug effects better (as the open and inactive state occupancies available for binding should match a hERG1a model's predictions better than a hERG1a/1b model). Yet, since the CiPA v1.0 model and the torsade metric were designed and optimised to work with physiological model A, we might expect it to predict risk better. One could conceivably fit the hERG1a binding data with physiological model B to obtain the binding parameters, then apply these binding parameters to physiological model A to predict changes to native I_{Kr} and therefore clinical risk. However, fewer assumptions would be needed if one directly performed voltage-clamp experiments on hERG1a/1b cell lines (Ríos-Pérez et al., 2021) when calibrating pharmacological binding models, as compounds with differing affinities for hERG1a and 1b have been observed (Abi-Gerges et al., 2011).

We further note the potential of using computational methods for studying molecular structural dynamics and relationships in drug binding, which may also provide insight into the binding mechanisms (DeMarco et al., 2021; Munawar et al., 2019; P.-C. Yang et al., 2020). In future, structural approaches could enhance our approach, in terms of ruling out further binding mechanisms, particularly when all voltage-dependent state structures for wild-type hERG1a and 1b are available (Abi-Gerges et al., 2011; Maly et al., 2022; Y. Zhang et al., 2020).

Finally, to our knowledge, this is the first study that attempts to address the question of whether we need a complex pharmacological model that attempts to nest most/all of these binding mechanisms or a set of multiple possible simpler pharmacological models to better represent *uncertainty* in proarrhythmic risk predictions. In theory, if parameter unidentifiability were not an issue, the two wings should arrive at the same conclusion—for example, when modelling an untrapped compound, the transition rates to the trapping component of the complex model would approach zero, and the non-trapping (simpler) model would be selected as the only plausible model. However, it may be better to use simpler (fewer parameter) models that can reproduce the underlying binding mechanism given the difficulty of eliciting information-rich data for calibrating one-size-fits-all complex binding models leading to potential parameter unidentifiability issues (Whittaker et al., 2020), given the inevitable presence of some model discrepancy (Lei, Ghosh, et al., 2020) and residual experimental artefacts (Lei, Clerx, et al., 2020). Pragmatically, we would suggest to select and use all the *plausible* simple models for prediction as demonstrated here—a type of ensemble model prediction which provides an estimate of uncertainty due to model discrepancy (Murphy et al., 2007; Parker, 2013; Tebaldi & Knutti, 2007).

In conclusion, this study has developed an approach to analyse a set of possible pharmacological small molecule binding models of hERG that is effective in assessing their impacts, as well as the impact of different physiological I_{Kr} models, on the proarrhythmic risk predictions. Determining the details of binding mechanisms, perhaps through the design of an improved calibration protocol, is crucial for mitigating the induced, substantial uncertainty in risk predictions for some compounds.

AUTHOR CONTRIBUTIONS

C. L. Lei, D. G. Whittaker, and G.R. Mirams conceptualised and designed the study. C. L. Lei and D. G. Whittaker wrote the code. C. L. Lei performed the simulations and data analysis and designed the visualisation and generated the results figures. C. L. Lei and G.R. Mirams wrote the manuscript. All authors revised and approved the final version of the manuscript.

ACKNOWLEDGEMENTS

We would like to thank a number of people who have helped to form our ideas on potential modes of hERG binding, in particular: Adam Hill, Jamie Vandenberg, Randall Rasmusson, Jules Hancox, Tom Claydon, Gail Robertson, Erick Rios Perez, Ken Wang, Derek Leishman, and Zhihua Li.

CONFLICT OF INTEREST STATEMENT

DGW is now an employee of GSK. GRM is a member of the CiPA Steering Committee.

DECLARATION OF TRANSPARENCY AND SCIENTIFIC RIGOUR

This Declaration acknowledges that this paper adheres to the principles for transparent reporting and scientific rigour of preclinical research as stated in the *BJP* guidelines for Design and Analysis, and as recommended by funding agencies, publishers, and other organisations engaged with supporting research.

DATA AVAILABILITY STATEMENT

The original electrophysiology data are available from the repository associated with Li et al. (2019) (https://bit.ly/fda-cipa-herg-milnes). The source code and data that support the findings of this study are openly available in GitHub at https://github.com/CardiacModelling/hERG-binding-mechanisms under a BSD 3-clause open source licence,

and a permanently archived version is available on Zenodo at https://doi.org/10.5281/zenodo.8325348.

ORCID

Chon Lok Lei https://orcid.org/0000-0003-0904-554X
Dominic G. Whittaker https://orcid.org/0000-0002-2757-5491
Gary R. Mirams https://orcid.org/0000-0002-4569-4312

REFERENCES

Abi-Gerges, N., Holkham, H., Jones, E. M. C., Pollard, C. E., Valentin, J. P., & Robertson, G. A. (2011). hERG subunit composition determines differential drug sensitivity. *British Journal of Pharmacology*, *164*, 419–432.

Alexander, S. P. H., Mathie, A., Peters, J. A., Veale, E. L., Striessnig, J., Kelly, E., Armstrong, J. F., Faccenda, E., Harding, S. D., Pawson, A. J., Southan, C., Davies, J. A., Aldrich, R. W., Attali, B., Baggetta, A. M., Becirovic, E., Biel, M., Bill, R. M., Catterall, W. A., & Zhu, M. (2021). The Concise Guide to PHARMACOLOGY 2021/22: Ion channels. *British Journal of Pharmacology*, *178*, S157–S245.

Beattie, K. A., Hill, A. P., Bardenet, R., Cui, Y., Vandenberg, J. I., Gavaghan, D. J., de Boer, T. P., & Mirams, G. R. (2018). Sinusoidal voltage protocols for rapid characterisation of ion channel kinetics. *The Journal of physiology*, *596*(10), 1813–1828.

Butler, A., Helliwell, M. V., Zhang, Y., Hancox, J. C., & Dempsey, C. E. (2020). An update on the structure of hERG. *Frontiers in Pharmacology*, *10*, 1572.

Carmeliet, E., & Mubagwa, K. (1998). Antiarrhythmic drugs and cardiac ion channels: Mechanisms of action. *Progress in Biophysics and Molecular Biology*, *70*(1), 1–72.

Clerx, M., Robinson, M., Lambert, B., Lei, C. L., Ghosh, S., Mirams, G. R., & Gavaghan, D. J. (2019). Probabilistic inference on noisy time series (PINTS). *Journal of Open Research Software*, *7*(1), 23.

Colquhoun, D., Dowsland, K. A., Beato, M., & Plested, A. J. R. (2004). How to impose microscopic reversibility in complex reaction mechanisms. *Biophysical Journal*, *86*, 3510–3518.

Curran, M. E., Splawski, I., Timothy, K. W., Vincen, G. M., Green, E. D., & Keating, M. T. (1995). A molecular basis for cardiac arrhythmia: hERG mutations cause long QT syndrome. *Cell*, *80*, 795–803.

DeMarco, K. R., Yang, P.-C., Singh, V., Furutani, K., Dawson, J. R. D., Jeng, M.-T., Fettinger, J. C., Bekker, S., Ngo, V. A., Noskov, S. Y., & Yarov-Yarovoy, V. (2021). Molecular determinants of pro-arrhythmia proclivity of d-and l-sotalol via a multi-scale modeling pipeline. *Journal of Molecular and Cellular Cardiology*, *158*, 163–177.

Dutta, S., Chang, K. C., Beattie, K. A., Sheng, J., Tran, P. N., Wu, W. W., Wu, M., Strauss, D. G., Colatsky, T., & Li, Z. (2017). Optimization of an in silico cardiac cell model for proarrhythmia risk assessment. *Frontiers in Physiology*, *8*, 616.

Escobar, F., Gomis-Tena, J., Saiz, J., & Romero, L. (2022). Automatic modeling of dynamic drug-hERG channel interactions using three voltage protocols and machine learning techniques: A simulation study. *Computer Methods and Programs in Biomedicine*, *226*, 107148.

Farm, H. J., Clerx, M., Cooper, F., Polonchuk, L., Wang, K., Gavaghan, D. J., & Lei, C. L. (2023). Importance of modelling hERG binding in predicting drug-induced action potentials for drug safety assessment. *Frontiers in Pharmacology*, *14*, 1110555.

Gomis-Tena, J., Brown, B. M., Cano, J., Trenor, B., Yang, P. C., Saiz, J., Clancy, C. E., & Romero, L. (2020). When does the IC50 accurately assess the blocking potency of a drug?. *Journal of Chemical Information and Modeling*, *60*, 1779–1790.

Han, S., Han, S., Kim, K.-S., Lee, H.-A., & Yim, D.-S. (2019). Usefulness of Bnet, a simple linear metric in discerning Torsades De pointes risks in 28 CiPA drugs. *Frontiers in Pharmacology*, *10*, 1419.

Hansen, N. (2006). The CMA evolution strategy: A comparing review. In Lozano, J. A., Larrañaga, P., Inza, I., & Bengoetxea, E. (Eds.), *Towards a new evolutionary computation: Advances in the estimation of distribution algorithms*. Heidelberg: Springer-Verlag, pp. 75–102.

Heist, E. K., & Ruskin, J. N. (2010). Drug-induced arrhythmia. *Circulation*, *122*(14), 1426–1435.

Hille, B. (1977). Local anesthetics: Hydrophilic and hydrophobic pathways for the drug-receptor reaction. *The Journal of General Physiology*, *69*(4), 497–515.

Hondeghem, L. M. (1987). Antiarrhythmic agents: Modulated receptor applications. *Circulation*, *75*, 514–520.

Hondeghem, L. M., & Katzung, B. G. (1977). Time-and voltage-dependent interactions of antiarrhythmic drugs with cardiac sodium channels. *Biochimica et Biophysica Acta (BBA)-Reviews on Biomembranes*, *472*(3-4), 373–398.

ICH (2005). S7B the non-clinical evaluation of the potential for delayed ventricular repolarization (QT interval prolongation) by human pharmaceuticals. International Council for Harmonisation of Technical Requirements for Pharmaceuticals for Human Use. Retrieved December 12, 2022, from https://database.ich.org/sites/default/files/S7B_Guideline.pdf

ICH (2022). E14 & S7B Questions and Answers: Clinical and Nonclinical Evaluation of QT/QTc Interval Prolongation and Proarrhythmic Potential. International Council for Harmonisation of Technical Requirements for Pharmaceuticals for Human Use. Retrieved December 12, 2022, fromhttps://database.ich.org/sites/default/files/E14-S7B_QAs_Step4_2022_0221.pdf

Jones, E. M. C., Roti, E. C. R., Wang, J., Delfosse, S. A., & Robertson, G. A. (2004). Cardiac IKr channels minimally comprise hERG 1a and 1b subunits. *Journal of Biological Chemistry*, *279*, 44690–44694.

Kamiya, K., Niwa, R., Mitcheson, J. S., & Sanguinetti, M. C. (2006). Molecular determinants of hERG channel block. *Molecular Pharmacology*, *69*, 1709–1716.

Kamiya, K., Niwa, R., Morishima, M., Honjo, H., & Sanguinetti, M. C. (2008). Molecular determinants of hERG channel block by terfenadine and cisapride. *Journal of Pharmacological Sciences*, *108*, 301–307.

Lee, W., Windley, M. J., Perry, M. D., Vandenberg, J. I., & Hill, A. (2019). Protocol-dependent differences in IC50 values measured in hERG assays occur in a predictable way and can be used to quantify state preference of drug binding. *Molecular Pharmacology*, *96*, 534867.

Lee, W., Windley, M. J., Vandenberg, J. I., & Hill, A. P. (2017). In vitro and in silico risk assessment in acquired long QT syndrome: The devil is in the details. *Frontiers in Physiology*, *8*, 934.

Lei, C. L., Clerx, M., Beattie, K. A., Melgari, D., Hancox, J. C., Gavaghan, D. J., Polonchuk, L., Wang, K., & Mirams, G. R. (2019). Rapid characterisation of hERG channel kinetics II: Temperature dependence. *Biophysical Journal*, *117*, 2455–2470.

Lei, C. L., Clerx, M., Gavaghan, D. J., & Mirams, G. R. (2023). Model-driven optimal experimental design for calibrating cardiac electrophysiology models. *Computer Methods and Programs in Biomedicine*, *240*, 107690.

Lei, C. L., Clerx, M., Gavaghan, D. J., Polonchuk, L., Mirams, G. R., & Wang, K. (2019). Rapid characterisation of hERG channel kinetics I: using an automated high-throughput system. *Biophysical Journal*, *117*, 2438–2454.

Lei, C. L., Clerx, M., Whittaker, D. G., Gavaghan, D. J., De Boer, T. P., & Mirams, G. R. (2020). Accounting for variability in ion current recordings using a mathematical model of artefacts in voltage-clamp experiments. *Philosophical Transactions of the Royal Society A*, *378*(2173), 20190348.

Lei, C. L., Ghosh, S., Whittaker, D. G., Aboelkassem, Y., Beattie, K. A., Cantwell, C. D., Delhaas, T., Houston, C., Novaes, G. M., Panfilov, A. V., & Pathmanathan, P. (2020). Considering discrepancy when calibrating a mechanistic electrophysiology model. *Philosophical Transactions of the Royal Society A*, *378*(2173), 20190349.

Lei, C. L., & Mirams, G. R. (2021). Neural network differential equations for ion channel modelling. *Frontiers in Physiology*, *12*, 1166.

Li, Z., Dutta, S., Sheng, J., Tran, P. N., Wu, W., Chang, K., Mdluli, T., Strauss, D. G., & Colatsky, T. (2017). Improving the in silico assessment of proarrhythmia risk by combining hERG (human Ether-à-go-go-Related Gene) channel-drug binding kinetics and multichannel pharmacology. *Circulation: Arrhythmia and Electrophysiology*, *10*, e004628.

Li, Z., Ridder, B. J., Han, X., Wu, W. W., Sheng, J., Tran, P. N., Wu, M., Randolph, A., Johnstone, R. H., Mirams, G. R., Kuryshev, Y., Kramer, J., Wu, C., Crumb, W. J., & Strauss, D. G. (2019). Assessment of an in silico mechanistic model for proarrhythmia risk prediction under the CiPA initiative. *Clinical Pharmacology & Therapeutics*, *105*, 466–475.

Maly, J., Emigh, A. M., DeMarco, K. R., Furutani, K., Sack, J. T., Clancy, C. E., Vorobyov, I., & Yarov-Yarovoy, V. (2022). Structural modeling of the herg potassium channel and associated drug interactions. *Frontiers in Pharmacology*, *13*, 966463.

Milnes, J. T., Witchel, H. J., Leaney, J. L., Leishman, D. J., & Hancox, J. C. (2010). Investigating dynamic protocol-dependence of hERG potassium channel inhibition at 37 °C: Cisapride versus dofetilide. *Journal of Pharmacological and Toxicological Methods*, *61*, 178–191.

Mirams, G. R., Cui, Y., Sher, A., Fink, M., Cooper, J., Heath, B. M., McMahon, N. C., Gavaghan, D. J., & Noble, D. (2011). Simulation of multiple ion channel block provides improved early prediction of compounds' clinical torsadogenic risk. *Cardiovascular Research*, *91*, 53–61.

Mistry, H. B. (2019). Comprehensive in vitro proarrhythmic assay complexity bias. *Clinical Pharmacology & Therapeutics*, *105*, 1323–1324.

Mitcheson, J. S. (2008). hERG potassium channels and the structural basis of drug-induced arrhythmias. *Chemical Research in Toxicology*, *21*, 1005–1010.

Mitcheson, J. S., Chen, J., & Sanguinetti, M. C. (2000). Trapping of a methanesulfonanilide by closure of the hERG potassium channel activation gate. *The Journal of General Physiology*, *115*, 229–240.

Montnach, J., Lorenzini, M., Lesage, A., Simon, I., Nicolas, S., Moreau, E., Marionneau, C., Baró, I., De Waard, M., & Loussouarn, G. (2021). Computer modeling of whole-cell voltage-clamp analyses to delineate guidelines for good practice of manual and automated patch-clamp. *Scientific Reports*, *11*(1), 3282.

Munawar, S., Vandenberg, J. I., & Jabeen, I. (2019). Molecular docking guided grid-independent descriptor analysis to probe the impact of water molecules on conformational changes of hERG inhibitors in drug trapping phenomenon. *International Journal of Molecular Sciences*, *20*(14), 3385.

Murphy, J. M., Booth, B., Collins, M., Harris, G. R., Sexton, D. M. H., & Webb, M. J. (2007). A methodology for probabilistic predictions of regional climate change from perturbed physics ensembles. *Philosophical Transactions of the Royal Society A: Mathematical, Physical and Engineering Sciences*, *365*, 1993–2028.

O'Hara, T., Virág, L., Varró, A., & Rudy, Y. (2011). Simulation of the undiseased human cardiac ventricular action potential: Model formulation and experimental validation. *PLoS Computational Biology*, *7*(5), e1002061.

Pareja, K., Chu, E., Dodyk, K., Richter, K., & Miller, A. (2013). Role of the activation gate in determining the extracellular potassium dependency of block of hERG by trapped drugs. *Channels*, *7*, 23–33.

Parker, W. S. (2013). Ensemble modeling, uncertainty and robust predictions. *WIREs Climate Change*, *4*, 213–223.

Raba, A. E., Cordeiro, J. M., Antzelevitch, C., & Beaumont, J. (2013). Extending the conditions of application of an inversion of the Hodgkin–huxley gating model. *Bulletin of mathematical biology*, *75*(5), 752–773.

Rennie, J. D. M., & Srebro, N. (2005). Loss functions for preference levels: Regression with discrete ordered labels, *Proceedings of the IJCAI Multidisciplinary Workshop on Advances in Preference Handling*. Menlo Park, CA: AAAI Press.

Ríos-Pérez, E. B., Liu, F., Stevens-Sostre, W. A., Eichel, C. A., Silignavong, J., & Robertson, G. A. (2021). A stable cell line inducibly expressing hERG1a/1b heteromeric channels. *Journal of Pharmacological and Toxicological Methods*, *110*, 107081.

Sager, P. T., Gintant, G., Turner, J. R., Pettit, S., & Stockbridge, N. (2014). Rechanneling the cardiac proarrhythmia safety paradigm: A meeting report from the cardiac safety research consortium. *American Heart Journal*, *167*(3), 292–300.

Sale, H., Wang, J., O'Hara, T. J., Tester, D. J., Phartiyal, P., He, J.-Q., Rudy, Y., Ackerman, M. J., & Robertson, G. A. (2008). Physiological properties of hERG 1a/1b heteromeric currents and a hERG 1b-specific mutation associated with Long-QT syndrome. *Circulation Research*, *103*(7), e81–e95.

Sanguinetti, M. C., Jiang, C., Curran, M. E., & Keating, M. T. (1995). A mechanistic link between an inherited and an acquird cardiac arrthytmia: HERG encodes the I_{Kr} potassium channel. *Cell*, *81*, 299–307.

Sanguinetti, M. C., & Tristani-Firouzi, M. (2006). hERG potassium channels and cardiac arrhythmia. *Nature*, *440*, 463–469.

Starmer, C. F., & Courtney, K. R. (1986). Modeling ion channel blockade at guarded binding sites: Application to tertiary drugs. *American Journal of Physiology-Heart and Circulatory Physiology*, *251*, H848–H856.

Starmer, C. F., Lastra, A. A., Nesterenko, V. V., & Grant, A. O. (1991). Proarrhythmic response to sodium channel blockade. theoretical model and numerical experiments. *Circulation*, *84*, 1364–1377.

Starmer, C. F., Nesterenko, V. V., Gilliam, F. R., & Grant, A. O. (1990). Use of ionic currents to identify and estimate parameters in models of channel blockade. *American Journal of Physiology-Heart and Circulatory Physiology*, *259*, H626–H634.

Stork, D., Timin, E. N., Berjukow, S., Huber, C., Hohaus, A., Auer, M., & Hering, S. (2007). State dependent dissociation of hERG channel inhibitors. *British Journal of Pharmacology*, *151*, 1368–1376.

Tebaldi, C., & Knutti, R. (2007). The use of the multi-model ensemble in probabilistic climate projections. *Philosophical Transactions of the Royal Society A: Mathematical, Physical and Engineering Sciences*, *365*, 2053–2075.

Thouta, S., Lo, G., Grajauskas, L., & Claydon, T. (2018). Investigating the state dependence of drug binding in hERG channels using a trapped-open channel phenotype. *Scientific Reports*, *8*(1), 1–9.

Thurner, P., Stary-Weinzinger, A., Gafar, H., Gawali, V. S., Kudlacek, O., Zezula, J., Hilber, K., Boehm, S., Sandtner, W., & Koenig, X. (2014). Mechanism of hERG channel block by the psychoactive indole alkaloid ibogaine. *Journal of Pharmacology and Experimental Therapeutics*, *348*, 346–358.

Vandenberg, J. I., Perry, M. D., Perrin, M. J., Mann, S. A., Ke, Y., & Hill, A. P. (2012). hERG K^+ channels: Structure, function, and clinical significance. *Physiological Reviews*, *92*, 1393–1478.

Veroli, G. Y. D., Davies, M. R., Zhang, H., Abi-Gerges, N., & Boyett, M. R. (2013). High-throughput screening of drug-binding dynamics to hERG improves early drug safety assessment. *American Journal of Physiology-Heart and Circulatory Physiology*, *304*, H104–H117.

Virtanen, P., Gommers, R., Oliphant, T. E., Haberland, M., Reddy, T., Cournapeau, D., Burovski, E., Peterson, P., Weckesser, W., Bright, J., van der Walt, S. J., Brett, M., Wilson, J., Millman, K. J., Mayorov, N., Nelson, A. R. J., Jones, E., Kern, R., Larson, E., Carey, C. J., van Mulbregt, P., & SciPy 1.0 Contributors (2020). SciPy 1.0: Fundamental algorithms for scientific computing in Python. *Nature Methods*, *17*, 261–272.

Whittaker, D. G., Clerx, M., Lei, C. L., Christini, D. J., & Mirams, G. R. (2020). Calibration of ionic and cellular cardiac electrophysiology models. *Wiley Interdisciplinary Reviews: Systems Biology and Medicine*, *12*(4), e1482.

Windisch, A., Timin, E. N., Schwarz, T., Stork-Riedler, D., Erker, T., Ecker, G. F., & Hering, S. (2011). Trapping and dissociation of propafenone derivatives in hERG channels. *British Journal of Pharmacology*, *162*(7), 1542–1552.

Windley, M. J., Abi-Gerges, N., Fermini, B., Hancox, J. C., Vandenberg, J. I., & Hill, A. P. (2017). Measuring kinetics and potency of hERG block for CiPA. *Journal of Pharmacological and Toxicological Methods*, *87*, 99–107.

Windley, M. J., Mann, S. A., Vandenberg, J. I., & Hill, A. P. (2016). Temperature effects on kinetics of KV11.1 drug block have important consequences for in silico proarrhythmic risk prediction. *Molecular Pharmacology*, *90*, 1–11.

Yang, P.-C., DeMarco, K. R., Aghasafari, P., Jeng, M.-T., Dawson, J. R. D., Bekker, S., Noskov, S. Y., Yarov-Yarovoy, V., Vorobyov, I., & Clancy, C. E. (2020). A computational pipeline to predict cardiotoxicity: From the atom to the rhythm. *Circulation Research*, *126*(8), 947–964.

Yang, T., Prakash, C., Roden, D. M., & Snyders, D. J. (1995). Mechanism of block of a human cardiac potassium channel by terfenadine racemate and enantiomers. *British Journal of Pharmacology*, *115*(2), 267–274.

Zhang, S., Zhou, Z., Gong, Q., Makielski, J. C., & January, C. T. (1999). Mechanism of block and identification of the verapamil binding domain to hERG potassium channels. *Circulation Research*, *84*(9), 989–998.

Zhang, Y., Dempsey, C. E., & Hancox, J. C. (2020). Electrophysiological characterization of the modified hERGT potassium channel used to obtain the first cryo-EM hERG structure. *Physiological Reports*, *8*(20), e14568.

SUPPORTING INFORMATION

Additional supporting information can be found online in the Supporting Information section at the end of this article.

How to cite this article: Lei, C. L., Whittaker, D. G., & Mirams, G. R. (2023). The impact of uncertainty in hERG binding mechanism on in silico predictions of drug-induced proarrhythmic risk. *British Journal of Pharmacology*, 1–18. https://doi.org/10.1111/bph.16250